Dynamics and thermal instability of magnetic flux in type-II superconductors

B. Ya. Shapiro,[1,*] I. Shapiro,[1] B. Rosenstein,[2] and F. Bass[1]
[1]*Department of Physics, Bar Ilan University, Ramat Gan 52100, Israel*
[2]*Department of Electrophysics, National Chiao Tung University, Hsinchu, Taiwan, Republic of China.*
(Received 8 June 2004; revised manuscript received 17 November 2004; published 17 May 2005)

In recent experiments, trapped magnetic flux is initially generated by abrupt laser heating of a strip of a type-II superconducting film subjected to a weak magnetic field. We study herein the nonequilibrium penetration of the flux into the Meissner state area. Effects of the heat dissipation and transport on the motion and stability of the interface between the magnetic flux and flux-free domains are considered. It is shown that the magnetic induction and the temperature have the form of a shock wave moving with constant velocity as large as that corresponding to the depairing current. In the vicinity of the front, superconductivity is suppressed by strong screening currents. The front velocity is determined by the Joule heat caused by the electric current in the normal domain at the flux front. The stability of the shock wave solution is investigated both analytically and numerically. For sufficiently small heat diffusion constant a finger shaped thermal instability is found.

DOI: 10.1103/PhysRevB.71.184508 PACS number(s): 74.20.De, 74.25.Ha, 74.25.Qt

I. INTRODUCTION

The dynamics of magnetic flux penetration into a type-II superconductor and its instabilities have been studied by a variety of techniques over the years, (see Ref. 1, and references therein). Magneto-optics experiments[2] demonstrate that in a wide range of situations there exists a well-defined interface (front) between the magnetic flux penetrating into the sample and the flux-free Meissner state. Improvements to these magneto-optical techniques have revealed a wide class of instabilities, including magnetic macroturbulence[3,4] and a dendritic instability.[5] The instability of the magnetic flux and flux avalanches are observed both in anisotropic high temperature superconductor[4] and in an isotropic material like Nb.[5]

Traditionally there are three possible scenarios in which the instabilities could arise. The standard thermomagnetic instabilities appear when the critical vortex state[6] is perturbed locally by the heat released by a moving vortex. This dissipation leads to the thermal softening of the vortex system which in turn is responsible for the instability.[1] In this case the instability develops around a well defined thermodynamically stable Bean state. There is no moving front in this case. A different type of thermal instability, namely the thermal overheating instability of the steady flux-antiflux front, was considered theoretically by some of us.[7] In this case the excess heat released at the front is caused by vortex-antivortex annihilation. Yet another type of instability occurs in strongly anisotropic superconductors.[8,9] In this case the stationary vortex-antivortex interface is destroyed by the Thomas-Kelvin instability.

Recently, a type of flux instability was observed experimentally. In these experiments superconductivity was locally destroyed in a completely nonadiabatic fashion by a femtosecond laser pulse.[10] The pulse clearly forces the system out of thermal equilibrium. The superconductivity is destroyed inside a narrow strip of a YBCO film subjected to a magnetic field perpendicular to the film. The field does not exceed the first critical field H_{c1}, so that initially fluxons cannot penetrate the rest of the sample. Therefore the magnetic flux initially fills the normal domain. Recovery of superconductivity occurs in two stages. Once the short pulse is over, the strip cools and the flux nucleates into a dense system of Abrikosov vortices. The characteristic time of that stage is microscopic, of order of the Ginzburg-Landau (GL) relaxation time (appearing in the time dependent GL equations) $t_{GL} \sim 10^{-10}$ s. This process has been studied by us some time ago[11] and we do not address this stage in the present paper since it was shown that no instability is originated at this stage.

On the larger (mesoscopic) time scale the rapidly created vortices are pushed into the superconducting part of the sample. The fluxons move very fast with velocities of order of 10^5 cm/s (in YBCO).[10] The flux flow currents, J, in this case are much higher than the critical current J_c typical for the thermodynamic Bean model critical state, but smaller (although not much smaller) than the depairing current J_d: $J_d > J \gg J_c$. Just after the vortex nucleation stage the magnetic flux forms a rapidly moving front. This highly nonequilibrium relaxation dynamics is very different from the essentially adiabatic dynamics of the critical state discussed earlier. The front line shape is not always stable: sometimes it dynamically develops dendriticlike structures.[12]

The existence of the sharp and typically straight front can be in principle understood in the framework of the theory of nonlinear magnetic flux diffusion.[13,14] Geshkenbein *et al.* considered the flux diffusion in the creep regime, while Shapiro *et al.*[14] considered the flux flow regime. In both cases the temperature gradient effects were neglected and no instability of the front was predicted, namely, it was shown that corrugation of the front line is unfavorable. The front velocity under these assumptions decreases with time.[14] However, corrugation of the front is typically caused by thermal effects,[1] hence, one expects that in the case of fast dynamics of the front, these effects are even more important.

In the present paper we study both numerically and analytically the dynamics of the nonadiabatically created magnetic flux in sufficiently thick (thickness larger than the magnetic penetration length) superconducting films. In particular, effects of dissipation and the heat transport on the motion

and stability of the flux front are considered. It is shown that the Joule heat released at the flux front can produce front propagation at constant velocity inside the type-II superconductor. Heating of the front by the moving magnetic flux is essential. We found that for certain voltage–current characteristics of the superconductor in its resistive state, the magnetic induction penetrating a flux-free superconductor forms a sharp front. Strong superconducting currents in the vicinity of the front suppress superconductivity in this area and create a normal domain at the front. The interface moves with *constant* velocity which is completely determined by the Joule heat released in the normal domain at the leading edge of the front. The straight front line shows an instability with respect to local temperature fluctuations. In fact an excessive local temperature at the front leads to excessive Joule heat released there and in turn increases the local front velocity in the area of the fluctuation. The hydrodynamical tangential instability of the flux front destroys the flat front. Numerical simulation of the exact set of nonlinear equations allows us to study the evolution of the instability and demonstrates the emergence and development of the corrugated interface.

II. MODEL AND BASIC EQUATIONS

A. Hydrodynamics of the vortex matter (for the slab geometry)

Let us consider a typical experimental situation (see Ref. 12), when a relatively thick (with thickness larger than magnetic penetration depth λ) type-II superconducting film is subjected to a weak external magnetic field ($B<B_{c1}$). The magnetic induction $\mathbf{B}$ therefore has only a z component $B_z \equiv B$ and all dependencies on the z coordinate can be neglected. The two dimensional vortex systems is described by the magnetic induction $B(\mathbf{r},t)$ and the temperature profile $T(\mathbf{r},t)$, where $\mathbf{r}=(x,y)$ is a two dimensional vector. To derive the hydrodynamic equations one starts from the continuity equation for the fluxon density $n(\mathbf{r},t)=\Sigma_a \delta[\mathbf{r}-\mathbf{r}_a(t)]$ and the flux current $I_i(\mathbf{r},t)=\Sigma_a v_i^a(t)\delta[\mathbf{r}-\mathbf{r}_a(t)]$. Here $i=x,y$ and $a=1,\ldots N$ labels the fluxons. The continuity equation

$$\frac{\partial n}{\partial t} = -\nabla_i I_i \tag{1}$$

supplemented by the constituent relation

$$I_i(\mathbf{r},t) = D_f(\mathbf{r},t)\nabla_i n(\mathbf{r},t) \tag{2}$$

leads to the flux diffusion equation

$$\frac{\partial n(\mathbf{r},t)}{\partial t} = -\nabla_i[D_f(\mathbf{r},t)\nabla_i n(\mathbf{r},t)]. \tag{3}$$

Since $n(\mathbf{r},t)=B(\mathbf{r},t)/\phi_0$, where ϕ_0 is the unit flux, the Maxwell equation

$$-\frac{1}{c}\frac{\partial B}{\partial t} = \varepsilon_{ij}\nabla_i E_j \tag{4}$$

leads to the identification $E_i=(c/\phi_0)\varepsilon_{ij}D_f(\mathbf{r},t)\nabla_j n(\mathbf{r},t)$, while ε_{ij} is the antisymmetric tensor. Since in the mixed state of the type-II superconductor $\mathbf{E}=R\mathbf{J}$, where $R(B,T)$ is the resistivity, one obtains $R=(4\pi/\phi_0^2)D_f$. The electric current density in turn is equal to $J_i=(c/4\pi)\varepsilon_{ij}\nabla_j B$. The flux diffusion equation then takes the form

$$\frac{4\pi}{c^2}\frac{\partial B}{\partial t} = \frac{\partial}{\partial x}\left[R\frac{\partial B}{\partial x}\right] + \frac{\partial}{\partial y}\left[R\frac{\partial B}{\partial y}\right]. \tag{5}$$

The function $R(B,T)$ will be phenomenologically defined in the next subsection. In the normal state the same equation applies with the normal state resistivity.

Now we turn to the heat transport equation, identical to the conventional normal state heat balance equation

$$C\frac{\partial T}{\partial t} = D\nabla^2 T + \mathbf{J}\cdot\mathbf{E}(B,T) - \gamma C(T-T_0). \tag{6}$$

Here C is the heat capacity and D is the heat diffusion constant, T_0 is the temperature of the cooling liquid with $\gamma = 1/t_r$ being the heat relaxation constant, when t_r the heat relaxation time. The first term on the right hand side is the heat conduction, the second is the Joule heat, and the third describes the heat exchange between the slab and the cooling liquid. The Joule heat term consists of two different contributions. In the mixed state it is dominated by the motion of the magnetic flux, while in the normal metal when the superconductivity is suppressed by the currents, one has usual Ohmic resistance losses.

In the geometry we consider (see Fig. 3), the dependence of both the temperature and the magnetic induction on z can be neglected. The magnetic induction is independent of z, since thickness of the thick film (slab) in the z direction is assumed to be larger than the magnetic penetration length λ, while the temperature is uniform in the z direction, despite the presence of the last term, since the thermal diffusion length is typically much larger than the film's thickness. The detailed argumentation is presented in Ref. 15.

B. Resistivity at high currents

As a rule, the nonlinear resistivity $R(J,B,T) \equiv E(J,B,T)/J$ in the mixed state of a type-II superconductor is a complicated function of magnetic field, current and temperature, see Fig. 1. In this work we will be interested mainly in resistivity at currents much larger than the critical current J_c, when the pinned vortices are released. The vortex resistivity grows quickly above J_c either exponentially or as a power $R\propto J^\mu$ with large μ. In this relatively low current regime the dependence of the resistivity on magnetic induction B is very smooth (roughly linear). However, when the current approaches the depairing current J_d the power μ becomes smaller and resistivity strongly depends on B.

Recently detailed measurements of the I–V characteristics of Nb films at high current density of order 10^6 A/cm^2 were performed.[16] Near the depairing current it has the form

$$R(B,T) = R_n(T)\left[\frac{J}{J_d(T,B)}\right]^\mu. \tag{7}$$

Here $R_n(T)$ is the normal state resistivity. The dependence of the depairing current J_d on magnetic field and temperature[16] can be fitted well by the following form:

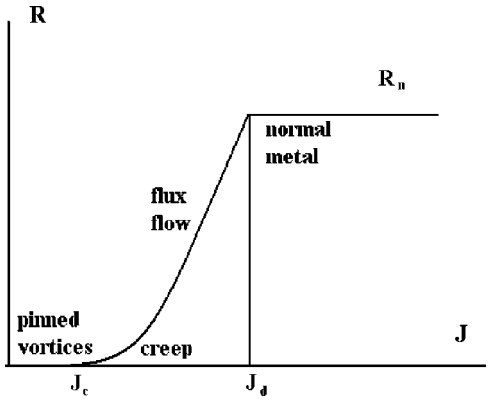

FIG. 1. Schematic plot of the nonlinear resistivity of a type-II superconductor in the mixed state as a function of current. The resistivity is zero below the critical current J_c, exponentially small in the flux creep regime just above J_c and evolves into a power function in the flux flow regime. At the depairing current it merges with the Ohmic normal state resistivity.

$$J_d(T,B) = J_{d0}\Delta\left[\frac{B_{c2}(T)}{B}\right]^{\nu/\mu}. \tag{8}$$

The upper critical field depends on temperature as $B_{c2}(T) = B_{c2}(0)\Delta$, where we assumed that dimensionless temperature $\theta = T/T_c$ is not far from 1, namely $\Delta \equiv 1-\theta$ is small.

When the current exceeds $J_d(B,T)$, the electric field is continuous, the resistivity saturates at its' normal value $R(B,T)=R_n(T)$. The derivative of R appearing in the nonlinear flux diffusion Eq. (5) is discontinuous. We fitted the I–V curves of Nb and obtained $\mu=1.5$ with temperature independent R_n. For Nb at fields of the order of B_{c1} we obtain the best fit $\nu=1.3$. The values of other material parameters are: $B_{c2}(0)=4.43$ T, $R_n=9.9$ $\mu\Omega$ cm and $T_c=8.6$ K. These were measured directly. The obtain the best fit for the constant $J_{d0}=9.2\cdot 10^6$ A/cm^2. See Fig. 2 for a sample of data taken at $T=7.8$ K, $\theta=0.9$.

Of course the exponents depend on material and weakly depend on field for larger magnetic fields. The power law however generally holds. Examples include YBCO well

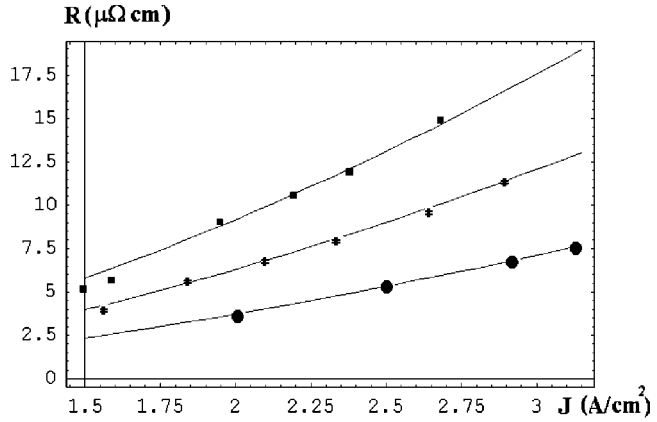

FIG. 2. A fit of the resistivity dependence on the current density of Ref. 16 to the model resistivity Eqs. (7),(8) with exponents $\nu=1.3$, $\mu=1.5$. Magnetic field is 20 mT (circles), 30 mT (stars) and 40 mT (squares).

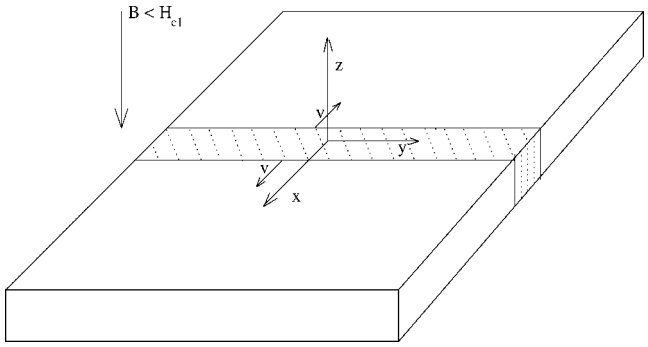

FIG. 3. The geometry of the problem. The dashed area contains the flux that penetrated the sample during the initial period in which superconductivity was destroyed in a narrow strip around $x=0$. The arrows marked with v indicate the direction of the flux front motion. The direction of the magnetic field B is perpendicular to the xy plane.

above B_{c1} (see Ref. 17) in which the power law is clearly seen, but $\mu=2$, $\nu=2$. The corresponding data on high T_c superconductors are not yet available for fields below B_{c1}, to our knowledge, and therefore we treat the powers as phenomenological parameters (see also Refs. 14 and 18). An additional difference between the conventional and the high T_c materials is that the normal state conductivity in high T_c cuprates is linear ("strange metal").

C. Boundary and initial conditions

In a typical experiment[12] the heat of the laser beam suppresses superconductivity in a narrow strip of width l dividing the sample into two equal superconducting parts of length L_x on both sides of the irradiated strip. Magnetic flux promptly fills the normal area and forms a nonequilibrium vortex strip state. Subsequently the laser is switched off and sample is cooled (see Fig. 3). The set of Eqs. (5) and (6) must be supplemented by the initial and boundary conditions in the center of the sample and on the sample's edges. The initial temperature is assumed to be homogeneous

$$T(x,y,t=0) = T_0, \tag{9}$$

where T_0 is the temperature of the cooling liquid. Magnetic field fills the irradiated area of width l and magnetic flux of magnitude

$$\Phi = 2lL_yB_0 = \int B(x,y,t)dxdy \tag{10}$$

is assumed to be trapped in superconductor and conserved. Here L_y is width of the sample. The boundary conditions for temperature are

$$T(x=\pm L_x, y=\pm L_y, t) = T_0. \tag{11}$$

An alternative boundary condition for the magnetic induction which we consider independently is fixed magnetic field at the center $B(x=0)=B_0$, while $B(x=\pm L_x)=0$.

D. Basic equations in terms of dimensionless quantities

Dimensionless coordinate, time, and magnetic induction are defined using natural units of length $x^*=cR_n(T=T_c)\equiv cR_n$, magnetic field $B^*=\sqrt{4\pi CT_c}$ and time

$$t^* = 4\pi R_n\left(\frac{4\pi R_n J_{d0}}{B^*}\right)^{\mu}\left[\frac{B_{c2}(0)}{B^*}\right]^{\nu} \tag{12}$$

as follows:

$$x \to x/x^*; \quad t \to t/t^*; \quad b = B/B^*. \tag{13}$$

For the free electron gas B^* is

$$B^* \approx H_{c1}\frac{\lambda^2 k_F v_F}{c\xi}, \tag{14}$$

where λ, k_F, v_F, and ξ are the London penetration length, Fermi momentum, Fermi velocity, and the coherence length respectively.

Using the scaled variables, the set of nonlinear coupled equations in the superconducting state $[J<J_d(B,T)]$ reads

$$\frac{\partial b}{\partial t} = \frac{\partial}{\partial x}\left(\rho\frac{\partial b}{\partial x}\right) + \frac{\partial}{\partial y}\left(\rho\frac{\partial b}{\partial y}\right), \tag{15}$$

$$\frac{\partial \theta}{\partial t} = \kappa\nabla^2\theta + \rho j^2 - \Gamma(\theta-\theta_0), \tag{16}$$

where the dimensionless resistivity and the electric current density are

$$\rho = \frac{R_n(\theta)}{R_n}\left(\frac{b}{\Delta}\right)^{\nu}\left(\frac{j}{\Delta}\right)^{\mu}; \quad j = \sqrt{\left(\frac{\partial b}{\partial x}\right)^2 + \left(\frac{\partial b}{\partial y}\right)^2} \tag{17}$$

and $\theta_0=T_0/T_c$. The unit of current density is $cB^*/4\pi x^*$. The flux diffusion equation does not contain parameters, while the heat transfer equation has two: the dimensionless temperature diffusion constant κ and the relaxation coefficient Γ:

$$\kappa = \frac{Dt^*}{Cx^{*2}}, \quad \Gamma = \gamma t^*. \tag{18}$$

In the region in which superconductivity is suppressed by the superconducting current J exceeding the depairing current value $J_d(B,T)$, the normal state resistivity becomes $R=R_n(T)$. In this case the basic equations are

$$\frac{\partial b}{\partial t} = \frac{\partial}{\partial x}\left(\rho_n\frac{\partial b}{\partial x}\right) + \frac{\partial}{\partial y}\left(\rho_n\frac{\partial b}{\partial y}\right), \tag{19}$$

$$\frac{\partial \theta}{\partial t} = \kappa\nabla^2\theta + \rho_n j^2 - \Gamma(\theta-\theta_0), \tag{20}$$

where the dimensionless normal state resistance is defined by

$$\rho_n(\theta) = R_n(\theta)\frac{c^2 t^*}{4\pi x^{*2}}. \tag{21}$$

In the following section we solve these equations both analytically and numerically.

III. STRAIGHT FLUX FRONT FOR $\mu=0$

A. Asymptotics in the superconducting phase

When the boundary conditions are independent of y (see notations in Fig. 3), the front is straight and the problem becomes one dimensional. We start with a case when the resistivity depends only on magnetic induction. Hence, now we consider $\mu=0$, returning to the general case in Sec. IV A. In addition we initially solve a simplified set dropping the relaxation term $\Gamma=0$ and diffusion $\kappa=0$. This assumption will be supported *a posteriori* by calculating the terms' effects and comparing with the numerical solution.

Looking for a solution of Eqs. (15) and (16) in the form

$$b = b_s(X), \quad \Delta = \Delta_s(X), \tag{22}$$

where $X=x-Vt$ is the distance from the interface and V is the interface velocity, one obtains

$$-V\frac{db_s}{dX} = \frac{d}{dX}\left[\left(\frac{b_s}{\Delta_s}\right)^{\nu}\frac{db_s}{dX}\right], \tag{23}$$

$$V\frac{d\Delta_s}{dX} = P_J. \tag{24}$$

Here the Joule power density is $P_J=\rho j^2$. Let us first investigate the asymptotics of $b_s(X)$ in the vicinity of the front $X\to 0$. In the cold superconductor, the magnetic field vanishes. Therefore formally (ignoring formation of the very narrow normal region near the front which will be discussed in the next subsection) we look at the magnetic field $b_s(X)$ as a power with coefficient dependent on velocity only for $X<0$:

$$b_s(X) = A(V)|X|^{\alpha}. \tag{25}$$

The temperature is assumed to be of the form

$$\Delta_s(X) = \Delta_{s0} - \Delta_{s1}(V)|X|^{\beta}. \tag{26}$$

Substituting the Ansatz Eqs. (25) and (26) into Eqs. (23) and (24), one obtains on the superconducting side of the front $(X<0)$:

$$VA\alpha|X|^{\alpha-1} = A^{\nu+1}\Delta_{s0}^{-\nu}\alpha[(\nu+1)\alpha-1]|X|^{(\nu+1)\alpha-2}, \tag{27}$$

$$A^{2+\nu}\alpha|X|^{2\alpha-2+\alpha\nu} = \Delta_{s1}\beta\Delta_{s0}^{\nu}V|X|^{\beta-1}, \tag{28}$$

which is satisfied for

$$\alpha = 1/\nu; \quad \beta = 2/\nu; \tag{29}$$

$$A(V) = \Delta_{s0}(\nu V)^{1/\nu}; \quad \Delta_{s1}(V) = \tfrac{1}{2}\Delta_{s0}^2(\nu V)^{2/\nu}. \tag{30}$$

The electric current $j=\partial b_s/\partial X$ formally diverges as $|X|^{1/\nu-1}$ at the front for $\nu>1$. Of course the divergence is intercepted by the phase transition into the normal state creating the "hot" region of presumably small width w_n determined by the condition that the depairing current is reached

$$j(X=-w_n) = j_d = \Delta_{s0}V(\nu V w_n)^{1/\nu-1}. \tag{31}$$

There is also dissipation in the superconducting part of a larger width w_s. The expression for the Joule heat term

caused by the magnetic flux motion everywhere, not necessarily close to the front interface, diverges at the front as [see Eq. (25)] $P_J \propto |X|^{2/\nu-1}$ for $\nu>2$ only. Its integral, however, always converges.

To determine V, w_n, and other characteristics of the front motion we need the solution in the normal domain. This and its matching with the asymptotics in the superconductor is considered next.

B. Solution in normal domain for the temperature independent resistivity

In the normal domain we assume first we assume for simplicity that $\rho_n(T)=\text{const}$ in addition to the previously used simplification $\kappa=\Gamma=0$. The nonlinear wave Ansatz

$$b = b_n(X), \quad \Delta = \Delta_n(X) \tag{32}$$

will be initially used to find the current density $j_n = (db_n/dX)$. Substitution of Eq. (32) into the normal state Eqs. (19) and (20) leads to the following set in terms of the front variable $X=x-Vt$:

$$-Vj_n = \rho_n \frac{dj_n}{dX}, \tag{33}$$

$$V\frac{d\Delta_n}{dX} = \rho_n j_n^2. \tag{34}$$

The first equation has a solution

$$j_n(X) = j_{n0}\exp\left[-\frac{XV}{\rho_n}\right] \approx j_{n0}\left(1-\frac{XV}{\rho_n}\right). \tag{35}$$

The approximate form is generally valid since $(|X|V/\rho_n) < (w_n V/\rho_n) \ll 1$ as will be justified *a posteriori*. Then the heat transfer equation and the boundary condition $\Delta_n(X=0) = \Delta_0$ gives

$$\Delta_n(X) = \Delta_0 - \frac{\rho_n j_{n0}^2}{2V^2}\left\{\exp\left[-\frac{2XV}{\rho_n}\right]-1\right\} \approx \Delta_0 + \frac{j_{n0}^2}{V}X. \tag{36}$$

In this region most of the heat is released

$$\Xi_n \equiv \int_{-w_n}^{0} \rho_n(\theta)\left(\frac{\partial b_n}{\partial X}\right)^2 dX \approx \rho_n j_n^2 w_n. \tag{37}$$

We will use this result later.

C. Matching solutions on the superconductor-normal interface and the flux front velocity

The current, temperature, and the temperature gradient are all continuous on the superconductor-normal interface located at $X=-w_n$. Consequently the current on the normal side approaches the same depairing current as that on the superconducting side, see Eq. (31). The temperature matching conditions are

$$\Delta(-w_n) = \Delta_0 - \frac{j_d^2 w_n}{V} = \Delta_{s0}, \tag{38}$$

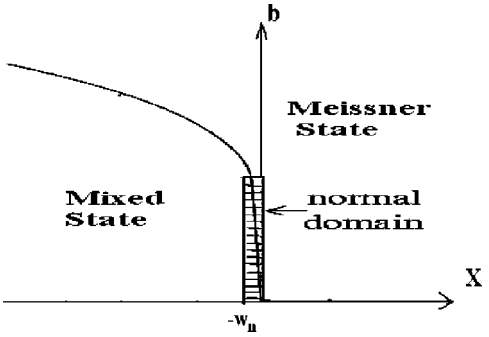

FIG. 4. The magnetic induction profile at the front. Three different regions, the mixed, the normal domain and the Meissner state are presented. Here w_n is the width of the normal domain in which superconductivity is suppressed by the high current, indicated by the hatched area at the leading edge of the front.

$$\Delta'(-w_n) = \frac{j_d^2}{V} = \frac{\Delta_{s0}^2}{\nu w_n}(\nu V w_n)^{2/\nu}. \tag{39}$$

The only solution of the set of three algebraic Eqs. (31), (38), and (39) is very simple

$$V = \frac{j_d}{2\Delta_0}\left[1+\sqrt{1+4\Delta_0/\nu}\right] \approx \frac{j_d}{\Delta_0}\left(1+\frac{\Delta_0}{\nu}\right), \tag{40}$$

$$w_n \approx \frac{\Delta_0}{\nu j_d}, \tag{41}$$

$$\Delta_{s0} \approx \Delta_0 - \frac{\Delta_0^2}{\nu}. \tag{42}$$

The front velocity is determined by the Joule heat released in the normal domain Eq. (37)

$$\Xi_n = \rho_n j_n^2 w_n = \frac{\rho_n j_d \Delta_0}{\nu} \tag{43}$$

as

$$V = \frac{\nu \Xi_n}{\rho_n \Delta_0^2}. \tag{44}$$

We will use this simple relation in numerical simulation described in the next subsection.

As we discuss later, the numerical results demonstrate that the width of the normal domain w_n (hatched area in Fig. 4) is much smaller than the width of the superconducting domain w_s in which the current is significant. When κ and Γ are nonzero only numerical analysis is possible. The results (see later) show that for reasonable values of κ and Γ the corresponding terms in the heat transfer equation are qualitatively insignificant. Of course in this case we cannot assume the simple form of Eq. (22).

D. The macroscopic description of the normal domain

Since the normal domain is very narrow, it is more convenient to avoid explicit matching in simulations treating

instead the heat release phenomenologically. In this approach the width of the normal domain is considered to be smaller than any other relevant scale and the normal part of the Joule heat term in the heat diffusion Eq. (16) is replaced by a delta function. This is equivalent to boundary condition on the front in which the normal domain contribution Ξ_n calculated in Eq. (43) is added. The fine structure of the front is ignored in such an approach but it still provides a simple relation between the temperature difference between the Meissner domain and the mixed state domain $[\theta]$,

$$V \simeq \frac{\Xi_n}{[\theta]}. \tag{45}$$

This is obtained by integration of the heat transfer Eq. (16) in the vicinity of the front.

The temperature jump at the front $[\theta]$ however cannot be calculated in the framework of such a simple phenomenological theory and has to be obtained from the microscopic theory [see Eq. (44)]. This allows us to relate the temperature jump across the front to the microscopic parameters of the problem

$$[\theta] = \frac{\rho_n \Delta_0^2}{\nu}, \tag{46}$$

where resistivity of the normal domain ρ_n is a parameter the microscopic model. This relation significantly simplifies the numerical simulation in which appearance of a singular shock wave naturally increases complexity. The simulation will go beyond the limit $\kappa=\Gamma=0$ treated analytically earlier.

E. Numerical solution for magnetic flux conserving boundary conditions

The set of the scaled one dimensional Eqs. (15) and (16) for resistivity in the form of Eq. (17) in the superconducting domain was solved numerically using the Euler method. The normal domain was not directly simulated and matched. Instead we used the phenomenological relations described in the previous subsection to set the boundary condition on the front. Parameters describing the, numerical "experiment" were chosen to be: $\mu=0$, $\nu=5$, $\Gamma=0$, and κ in the range 0.01–0.1. Size of the system is $L_x/x^*=200$. The boundary conditions are: the total flux $\Phi/(B^*x^{*2})$ in the range 0.5–2.5, temperature of the cold superconductor $\theta_0=0.7$:

$$\theta(x=-200)=\theta(x=200)=\theta_0. \tag{47}$$

The normal phase was not simulated since it can be integrated analytically. The transition to the normal state at depairing current was taken into account by holding constant the normal domain Joule heat dissipation Ξ_n for values in the range $5\cdot10^{-2}$–2.

The results of the numerical solution are presented in Figs. 5–7. The evolution of the magnetic induction is presented in Fig. 5 for the following values of the flux and heat diffusion constant: (a) $\Phi=0.5$, $\kappa=0.1$, (b) $\Phi=0.5$, $\kappa=0.01$, and (c) $\Phi=2.4$, $\kappa=0.05$. The value of Ξ_n was kept fixed at $\Xi_n=0.5$. Different curves represent successive times with intervals of $\Delta t=2.5t^*$ between them. Velocity of the sharp front

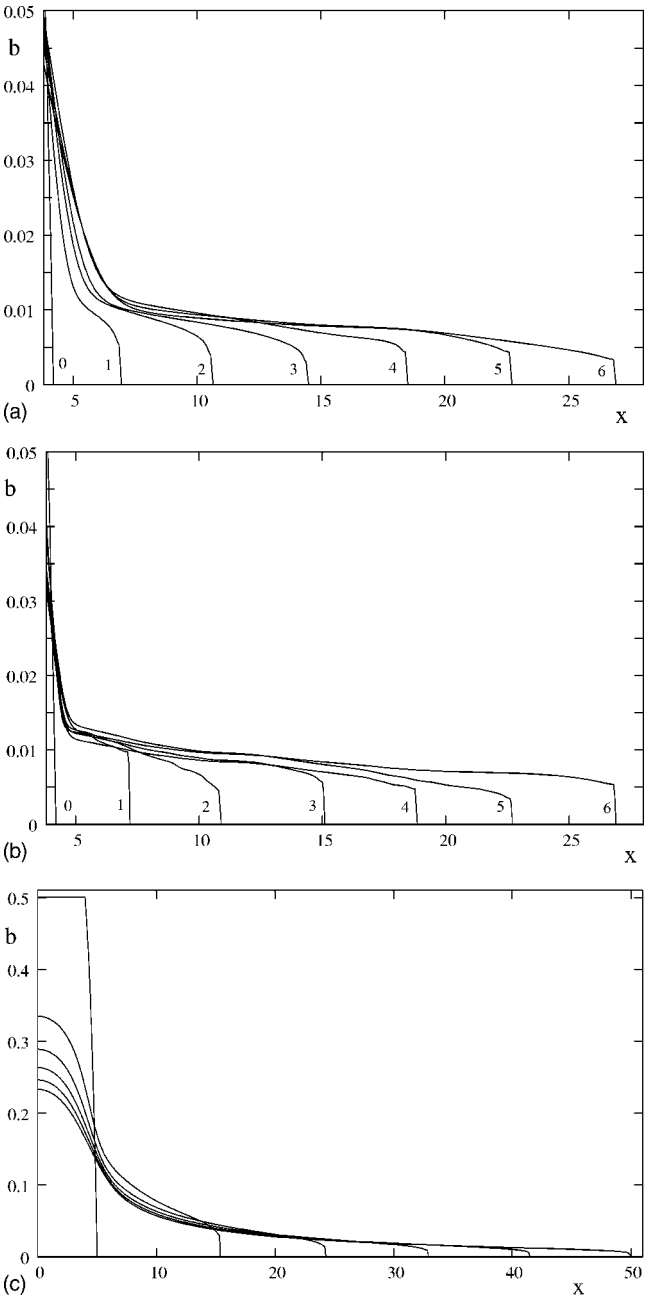

FIG. 5. The evolution of the magnetic induction for the flux conserving boundary condition. The value of the Joule heat released in the normal domain Ξ_n was kept fixed at $\Xi_n=0.5$. The curves correspond (from left to right) to six different times with intervals of Δt between them. (a) The flux $\Phi=0.5$ and the heat diffusion constant $\kappa=0.1$, $\Delta t=2.5\ t^*$. (b) $\Phi=0.5$, $\kappa=0.01$, $\Delta t=2.5\ t^*$. (c) $\Phi=2.4$, $\kappa=0.05$, $\Delta t=5\ t^*$.

is constant and is plotted as a function of Ξ_n in Fig. 6 for $\Phi=2.4$ and $\kappa=0.05$. The temperature front moves together with the flux front velocity. The data are presented for the same times as for the magnetic induction. It demonstrates that the front interface velocity V is linearly dependent on Ξ_n. The dependence of Φ is negligible. The results closely follow Eq. (44) obtained analytically for $\kappa=0$ and confirms the general physical picture proposed in the previous section that the velocity of the shock wave is universal in a sense

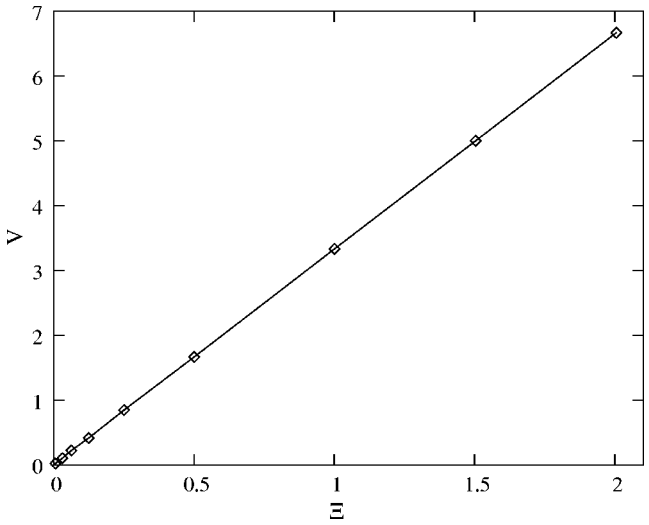

FIG. 6. Front velocity as a function of the Joule heat released in the normal domain Ξ_n. Here the flux is $\Phi=2.4$, the heat diffusion constant is $\kappa=0.05$. Squares correspond to the simulated values of Ξ_n, while the straight line is the analytical result.

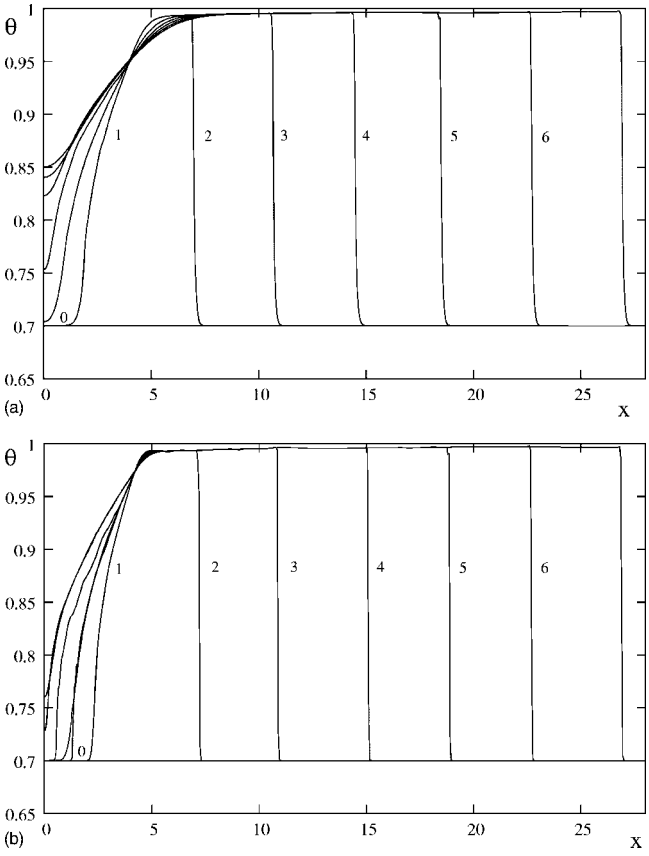

FIG. 7. The evolution of the temperature profile for the flux conserving boundary condition. The value of the Joule heat released in the normal domain. Ξ_n was kept fixed at $\Xi_n=0.5$. The curves correspond to six different times with intervals of $\Delta t=2.5\ t^*$ between them. (a) The flux $\Phi=0.5$ and heat diffusion constant is $\kappa=0.1$. (b) $\Phi=0.5$, $\kappa=0.01$.

that it depends only the heat released in the normal domain. The simulation reveals that the evolution is qualitatively the same for other values of the parameters.

The dynamics of the temperature distribution $\theta(x,t)$ is presented in Fig. 7 and has a form of a thermal shock wave. Two sets of parameters were simulated: (a) $\Phi=0.5$, $\kappa=0.1$, and (b) $\Phi=0.5$, $\kappa=0.01$. The maximum of temperature θ in this wave is reached at the interface between the superconducting and normal domains in the vicinity of the magnetic flux front. As we discussed in the previous section, the current is maximal in the normal domain which is narrow. We found in all the cases studied that the Joule heat released in the mixed state domain (see Fig. 4) does not exceed 1% of that in the normal domain. Note a curious feature of Fig. 7 that all the curves intersect at a certain point.

IV. GENERALIZATIONS: THE $\mu\neq 0$ RESISTIVITY AND THE CONSTANT MAGNETIC FIELD BOUNDARY CONDITION

A. More general *I–V* $\mu\neq 0$

Although in real samples resistance in the resistive mixed state might be a more complicated function than it was assumed earlier, the model representation in the form of Eqs. (7) and (8) with arbitrary critical exponents ν and μ is a robust and experimentally justified way to treat the problem. In such a case the main conclusions obtained for resistance with $\mu=0$, remain valid for some special relations between the critical exponents only.

Assuming b_s and Δ_s in the vicinity of the front ($X\rightarrow 0$) in the form of the Eqs. (25) and (26) one obtains asymptotically for $A(V)$ and α:

$$\alpha=\frac{\mu+1}{\nu+\mu};\quad A(V)=\Delta_{s0}V^{1/(\nu+\mu)}\left(\frac{\mu+1}{\mu+\nu}\right)^{-(\mu+1)/(\mu+\nu)}. \tag{48}$$

The electric current now behaves as

$$j\propto |X|^{(1-\nu)/(\mu+\nu)} \tag{49}$$

and still diverges for $\nu>1$. This condition is independent of μ, although the power in Eq. (49) depends on μ. In the case $\nu<1$ there is no normal domain and one can neglect the Joule heat. Hence, the temperature gradients are small and it suffices to consider the flux dynamics described by Eq. (15) with temperature fixed at θ_0. Looking for an exact solution in a form

$$b=b_1 t^{-\alpha} f(\zeta), \tag{50}$$

where $\zeta=b_2 x/t^{\beta}$, we obtain for b_1 and $f(\zeta)$ (see Refs. 7 and 19), under the flux conservation law boundary condition $\Phi=\int dx b(x,t)$:

$$\alpha=\beta=1/(2\mu+2+\nu);\quad b_1=\Phi^{(\mu+2)/(2\mu+2+\nu)};$$

$$b_2=\Phi^{-(\nu+\mu)/(2\mu+2+\nu)},$$

$$f(\zeta) = \left\{ \left(\frac{\mu+\nu}{\mu+2} \right) \left(\frac{1}{2\mu+2+\nu} \right)^{1/(\mu+1)} \zeta_f^{(\mu+2)/(\mu+1)} \times \left[1 - \left(\frac{\zeta}{\zeta_f} \right)^{(\mu+2/\mu+1)} \right] \right\}^{(1+\mu/\mu+\nu)}, \quad (51)$$

$$\zeta_f^{-(2\mu+\nu+2/\mu+\nu)} = \frac{\mu+1}{\mu+2} \left(\frac{\mu+\nu}{\mu+2} \right)^{((\mu+1/\mu+\nu)} \frac{1}{[2+2\mu+\nu]^{1/(\nu+\mu)}} \times \mathbf{B} \left[\frac{2+2\mu+\nu}{\mu+\nu}, \frac{\mu+1}{\mu+2} \right], \quad (52)$$

where **B** is the beta function. The flux front moves with velocity $V_f(t) = dx_f/dt \propto t^{\beta-1}$ decaying with time. In the absence of the excessive heat released at the flux front the flux front in this case is completely stable.

B. Constant magnetic field

In certain cases similar phenomena will occur when flux is not conserved. Examples include narrow stripes, fields larger than H_{c1}, etc. This does not mean that the effect disappears since magnetic flux generally forms a thermomagnetic shock wave. The main prerequisite is a phase transition from superconductor to normal metal resulting in a sharp flux front. This case was studied numerically for constant magnetic field (in units of B^*) $b=0.05$ and parameters $\nu=5$, $\kappa=0.05$, $\Gamma=0$, and $\Xi=0.5$. The profile of the magnetic field and the temperature shock waves are presented in Figs. 8(a),8(b), where different curves correspond (from left to right) to various times: $t=0$, 5, 10, 15… (in the t^* units). It is important to note that, when the simulation was done for different Ξ, the dependence was linear like for the constant flux in Fig. 6. This is consistent with our analytic result predicting that the front velocity is governed solely by the Joule heat released in the normal domain. Other features are also independent of boundary conditions.

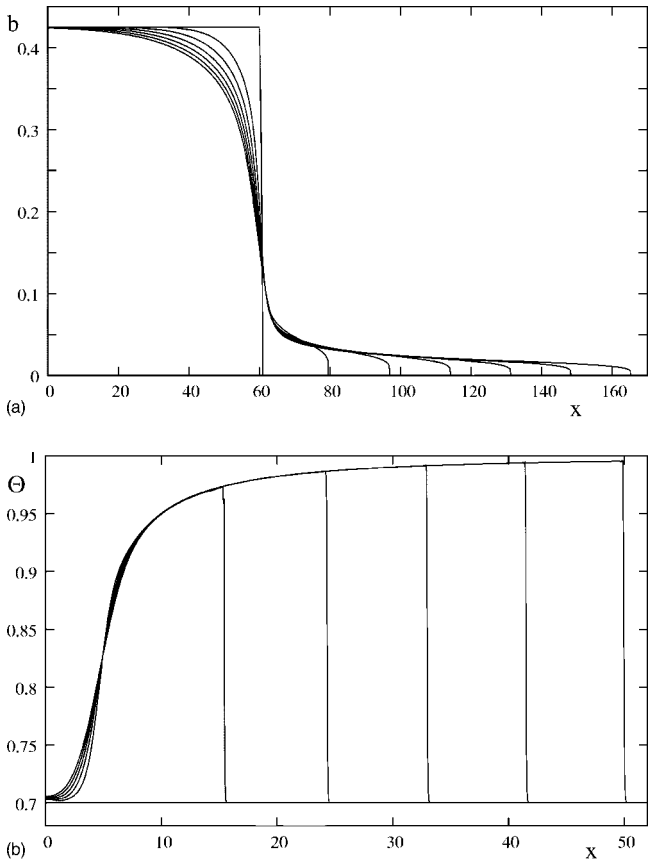

FIG. 8. Magnetic field at $x=0$ is constant. The curves correspond to six different times from left to right with intervals of $\Delta t = 5\ t^*$ between them. Joule heat released at the front $\Xi=0.5$. (a) The magnetic induction evolution and (b) the temperature shock wave.

V. INSTABILITY OF THE STRAIGHT FRONT

A. Linear stability analysis for $\kappa=\Gamma=0$

The dependence of the front velocity on the Joule heat released near the interface can lead to an instability of the straight front. Perturbations like a slight spatial distribution of the sample parameters (resistance, for example) can trigger the front instability. Keeping the normal resistivity in the form $\rho_n=\rho_0+\rho_1\theta(x,t)$ we look for a solution of the corrugated front in the normal domain as

$$b = b_n(x - Vt) + \eta(x,y,t),$$

$$\theta = \theta_n(x - Vt) + \zeta(x,y,t). \quad (53)$$

The leading order solution β_n and θ_n for the set of basic Eqs. (15) and (16) for $\rho_1=0$ were obtained in Sec. III, while corrections to the first order in ρ_1 will not be required in the stability analysis. The first order terms in perturbations η and ζ are

$$\frac{\partial \eta}{\partial t} = \rho_n(\theta_n)\nabla^2\eta + \rho_1 \frac{\partial \theta_n}{\partial x}\frac{\partial \eta}{\partial x} + \rho_1 \frac{\partial^2 b_n}{\partial x^2}\zeta + \rho_1 \frac{\partial b_n}{\partial x}\frac{\partial \zeta}{\partial x}, \quad (54)$$

$$\frac{\partial \zeta}{\partial t} = 2\rho_n(\theta_n)\frac{\partial b_n}{\partial x}\frac{\partial \eta}{\partial x} + \rho_1 \left(\frac{\partial b_n}{\partial x} \right)^2 \zeta. \quad (55)$$

Due to translation invariance of these eigenvalue equations in time and the direction along the front y one represents η, ζ in a form

$$\eta = \eta(x)\exp(\Omega t + k_y y); \quad \zeta = \zeta(X)\exp(\Omega t + k_y y). \quad (56)$$

Then the eigenvalue equations become one dimensional

$$\hat{L} \begin{bmatrix} \eta \\ \zeta \end{bmatrix} = \Omega \begin{bmatrix} \eta \\ \zeta \end{bmatrix}, \quad (57)$$

where

$$\hat{L}=\begin{array}{|c|c|}\hline \rho_n(\theta_n)\left(\frac{\partial^2}{\partial X^2}+\rho_1\frac{\partial\theta_n}{\partial X}\frac{\partial}{\partial X}-k_y^2\right) & \rho_1\left(\frac{\partial b_n}{\partial X}\frac{\partial}{\partial X}+\frac{\partial^2 b_n}{\partial X^2}\right)\\ \hline 2\rho_n(\theta_n)\frac{\partial b_n}{\partial X}\frac{\partial}{\partial X} & \rho_1\left(\frac{\partial b_n}{\partial X}\right)^2\\ \hline\end{array}. \tag{58}$$

Let us first consider the simpler case of conventional superconductors for which $\rho_1=0$. Substituting Eqs. (35),(36) into Eqs. (54) and (55) one obtains [replacing $(\partial/\partial X)\rightarrow ik_X$]:

$$\hat{L}_0=\begin{array}{|c|c|}\hline -\rho_0\left(k_X^2+k_y^2\right) & 0\\ \hline -2i\rho_0 j_d k_X & 0\\ \hline\end{array}. \tag{59}$$

The matrix $\hat{L}_0$ has one stable $\Omega_1=-\rho_0(k_X^2+k_y^2)$ and one marginal $\Omega_2=0$ eigenvalues. This eigenvalue is highly degenerate: any temperature deviation ζ for $\eta=0$ belongs to this subspace: $\hat{L}_0\left[\begin{smallmatrix}0\\ \zeta\end{smallmatrix}\right]=0$. Strictly speaking the marginal eigenvalue Ω_2 calls for investigation beyond the linear stability analysis. However, we believe it is stable and, in any case, addition of the ρ_1 term to resistivity removes the marginality and the degeneracy. To find the corrected eigenvalue Ω_2, one has to diagonalize on the corresponding subspace the operator

$$\hat{L}_{\zeta\zeta}=\rho_1\left(\frac{\partial b_n}{\partial X}\right)^2. \tag{60}$$

The derivative is nearly constant in the normal domain, see Eq. (35):

$$\hat{L}_{\zeta\zeta}=\rho_1 j_{n0}^2\exp\left[-\frac{2XV}{\rho_n}\right]\approx\rho_1 j_d^2. \tag{61}$$

Consequently

$$\Omega_2=\rho_1 j_d^2, \tag{62}$$

which demonstrates the instability for any wave vector.

The physical reason for the instability is the positive feedback between temperature fluctuation at the front increasing in its turn both the Joule power at the front and its velocity. In fact, it is the well known hydrodynamics tangential instability[20] of the flux front which is responsible for the front instability. Indeed, in this case warmer segments of the front move faster and can destroy the flat front line.

B. Stability in the general case: Numerical simulation

If the normal resistivity of the sample is temperature dependent and $\kappa=\Gamma=0$, then the normal domain in the front shows instability with respect to small temperature fluctuations with arbitrary wave vector. In this case the normal domain in the front shows instability with respect to small temperature fluctuations with arbitrary wave vectors. The dispersion appears for the nonzero heat diffusion coefficient. In fact, however, these small fluctuations cannot destroy the straight line front. It becomes unstable due to large amplitude fluctuations. Let us consider the evolution of the instability. First of all the instability can develop when the characteristic time $t_0\simeq 1/(\rho_1 j_d^2)$ is smaller than the characteristic time of the heat absorption in the sample $t_r\approx\Gamma^{-1}$. In addition the heat diffusion along the y axis can also affect the unstable fluctuations. In the latter case the requirement is: $ut_0>\sqrt{\kappa t_0}$. These two requirements allow us to determine the critical velocity of the fluctuation for the onset of the instability

$$u>u_c=\min\{\Gamma w_n, j_d\sqrt{\kappa\rho_1}\}. \tag{63}$$

In metals and alloys the normal state resistivity practically does not depend on temperature in the relevant temperature range. This means that $\rho_1=0$ and consequently no instability is expected.

The threshold in the fluctuation velocity u_c (which is proportional to the Joule heat released in the front) means that only a large temperature fluctuation can provide Joule heating necessary to destroy the planar front. Physically large amplitude fluctuations of the temperature at the front are nonuniform because they are caused by the spatial distribution of the impurities in the sample locally increasing resistivity and hence the Joule heat and velocity of the fluctuations in the front. Numerical simulations support this scenario.

In order to study the development of the instability for arbitrary κ, the set of the Eqs. (15),(16) have been solved numerically. The Joule heat power Ξ_n released in the normal domain at the front has the following model form:

$$\frac{\Xi_n(\theta)}{\Xi_{n0}}\equiv\frac{\rho_n(\theta)}{\rho_0}=1+\alpha[\theta(x,y,t)-\theta_0], \tag{64}$$

where initial temperature is perturbed in the region $0<x<5$, $4<y<5$, (temperature fluctuation $\theta(x,y,t=0)=0.88$), while outside this region $\theta(x,y,t=0)=\theta_0=0.7$. We chose $\alpha=14.5$, $\kappa=0.05$ and 2.5. Physically this kind of fluctuation represents a local variation of the normal state resistivity (proportional to Ξ_n) when the front of the shock wave passes an inhomogeneity.

The evolution of a small fluctuation in two opposite limits is presented in Fig. 9. For small κ, Fig. 9(a), an unstable pattern of the magnetic induction develops. It should be noted that the flux front line lost its stability essentially immediately after the temperature fluctuation affected the system. For finite κ we observe that most of the $\kappa=0$ unstable modes are diffused away and do not develop into an instability of the system. For large κ, Fig. 9(b), a similar perturbation relaxes into a straight line front and disappears in accord with the stability analysis.

VI. DISCUSSION

To summarize, we considered the formation and stability of the shock waves in the vortex matter under extreme conditions of the fast flux expansion into the Meissner state. In this case very strong screening currents significantly exceeding the critical current J_c flow in the mixed state. For such strong currents the vortex matter resistivity R has a form $R\propto B^\nu J^\mu$. We predict that when $\nu>1$ both the moving flux and the temperature profile form a sharp singular shock waves.

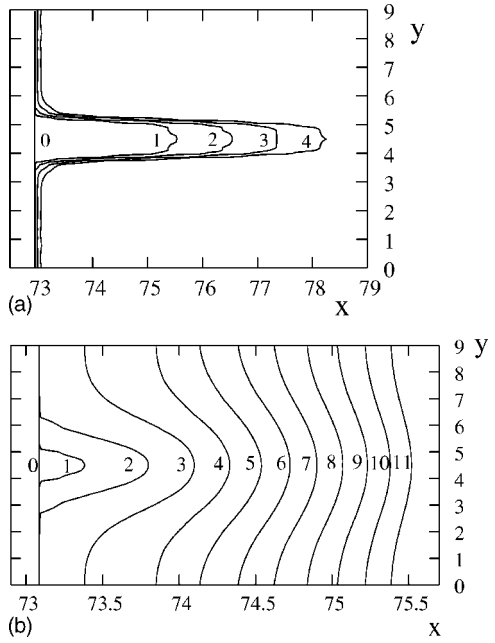

FIG. 9. Evolution of the magnetic flux front pattern for different values of the heat diffusion constant. The perturbation is triggered by the temperature inhomogeneity specified in Eq. (64). (a) Small heat diffusion constant $\kappa=0.05$. Development of the avalanche instability. Five snapshots (intervals of $\Delta t=0.05\ t^*$) of a finger shaped instability in magnetic induction are shown from left to right. (b) Large heat diffusion constant $\kappa=2.5$. Evolution of the magnetic flux pattern. The five snapshots (intervals of $\Delta t=0.125\ t^*$) show that the initial small fluctuation dissipates away.

Strong screening currents in the vortex matter approaching the depairing current J_d cause destruction of superconductivity. An area of material adjacent to the interface between the Meissner state and the mixed state of the size (returning to dimensional units) $W_n=[cB^*(1-T_0/T_c)/4\pi\nu J_{d0}]$ becomes normal. Here $B^*=\sqrt{4\pi CT_c}$, C is the heat capacity and T_0 is temperature of the cool superconductor. The stable superconductor-normal interface is formed due to combined effect of the nonlinear magnetic flux dynamics and thermal effects. The condition $\nu>1$ is independent on μ and has the following physical meaning. It is well known that above the critical current resistivity is proportional to the number of vortices (the flux flow Bardeen-Stephen formula), $R\propto B(\ \nu=1)$. The condition for formation of the normal domain is therefore that the dependence on magnetic induction at currents close to the depairing currents is stronger than linear. As was shown in Sec. II B for Nb, this happens at least for small fields.

The interface moves with constant velocity, which is completely determined by the Joule heat released in the normal domain at the front and hence on the normal resistivity of the sample. The flux front velocity has the form for $\mu=0$ (in dimensional units) is $V=[cR_nJ_{d0}/(1-T_0/T_c)B^*]\times[B^*/B_{c2}(0)]^\nu$. Taking for example material parameters of the optimally doped YBCO, $J_{d0}=10^8$ A/cm^2, $R_n=2\cdot10^{-6}\ \Omega$ cm, $C=1$ J/cm^3 K,[21] one obtains for the flux front velocity $V\approx10^5$ cm/s, which is in a good agreement with experimental data.[12] Note, however, that the value strongly depends on the exponents μ and ν. The width of the normal stripe is 0.5 μm.

The type of the voltage–current characteristic therefore is the decisive factor determining the flux front stability in type-II superconductors. The instability is developed when the voltage–current characteristics of the uniform superconductor in its resistive state provides sufficient screening currents at the moving flux front interface. The physical reason for the instability is very similar to a well known hydrodynamic instability,[20] when different layers of the liquid move with different and parallel velocities. In fact it is the positive feedback between excessive local temperature at the front and Joule heat released there that leads to instability. The hydrodynamic tangential instability of the flux front destroys the flat front. The instability develops for the fluctuation velocities exceeding the critical value $U>U_c=\min\{[cB^*(1-T_0/T_c)/4\pi\nu J_{d0}t_r],(J_{d0}/C)\sqrt{D\,(dR_n/dT)|_{T_c}}\}$, where D is the heat diffusion constant and t_r is the heat absorption time. Taking $D=30$ J/(cm s K) and $t_r=10^{-11}$ s, one estimates the two velocities as $5\cdot10^6$ cm/s and $2.6\cdot10^5$ cm/s.

The avalanche-type instability appears when the moving flux front enters the area in which locally the normal resistivity is large. The experimental observation of the fast flux dynamics in YBCO has been carried out by Leiderer *et al.*[12] The velocity of the front indeed has the universal character on the advanced stage of the instability and does not depend on initial magnetic gradients. The dendrite velocity in the later stages of disintegration of the front are expected to be of order of U_c. This instability is not expected to arise in materials like Nb since $dR_n/dT|_{T_c}$ is negligibly small and U_c vanishes.

ACKNOWLEDGMENTS

We are grateful to D. Kessler, Y. Yeshurun, Y. Rabin, A, Shaulov, and H. H. Wen for discussions and V. Vinokur for his criticism. This work was supported by The Israel Science Foundation, ESF Program "Cosmology in the Laboratory." We are also grateful to the Binational Israel-USA and Germany-Israel Foundations for support and to the Inter-University Computational Center for providing Cray J932 supercomputer facilities. B.R. acknowledges Albert Einstein Minerva Center for Theoretical Physics in Weizmann Institute and NSC grant ROC94-2112-M009-024 of R.O.C. and the hospitality of Bar Ilan University.

*Author to whom correspondence should be addressed.

[1] R. G. Mints and A. I. Rahmanov, Rev. Mod. Phys. **53**, 551 (1981); A. V. Gurevich, R. G. Mints, and A. I. Rahmanov, *The Physics of Composite Superconductors* (Begell House, NY, 1997).

[2] L. A. Dorosinskii, M. V. Indenbom, V. I. Nikitenko, Yu. A. Ossipyan, A. A. Polanskii, and V. K. Vlasko-Vlasov, Physica C **203**, 149 (1992).

[3] V. K. Vlasko-Vlasov, V. I. Nikitenko, A. A. Polyanskii, G. M. Crabtree, U. Welp, and B. W. Veal, Physica C **222**, 361 (1994).

[4] M. E. Gaevski, T. H. Johansen, Yu. Galperin, H. Bratsberg, A. V. Bobyl, D. V. Shautsev, and S. F. Karmarenko, Appl. Phys. Lett. **71**, 3147 (1997).

[5] C. A. Duran, P. L. Gammel, R. E. Miller, and D. J. Bishop, Phys. Rev. B **52**, 75 (1995).

[6] C. P. Poole, H. A. Farrah, and R. J. Creswick, *Superconductivity* (Academic Press, San Diego, 1995).

[7] F. Bass, B. Ya. Shapiro, and M. Shvartser, Phys. Rev. Lett. **80**, 2441 (1998).

[8] A. Gurevich, Phys. Rev. B **46**, 3638 (1992).

[9] L. M. Fisher, P. E. Goa, M. Baziljevich, T. H. Johansen, A. L. Rakhmanov, and V. A. Yampol'skii, Phys. Rev. Lett. **87**, 247005 (2001).

[10] P. Leiderer, J. Boneberg, P. Brull, V. Bujok, and S. Herminghaus, Phys. Rev. Lett. **71**, 2646 (1993); U. Bolz, J. Eisenmenger, J. Schiessling, B.-U. Runge, and P. Leiderer, Physica B **284-288**, 757 (2000); U. Bolz, D. Schmidt, B. Biehler, B.-U. Runge, R. G. Mints, K. Numssen, H. Kinder, and P. Leiderer, Physica C **388-389**, 715 (2003).

[11] I. Shapiro, E. Pechenik, and B. Ya. Shapiro, Phys. Rev. B **63**, 184520 (2001).

[12] U. Bolz, B. Biehler, D. Schmidt, B. U. Runge, and P. Leiderer, Europhys. Lett. **64**, 517-523 (2003).

[13] V. M. Vinokur, M. V. Feigelman, and V. B. Geshkenbein, Phys. Rev. Lett. **67**, 915 (1991).

[14] F. Bass, B. Ya. Shapiro, I. Shapiro, and M. Shvartser, Physica C **297**, 269 (1998); **297**, 269 (1998).

[15] F. Bass, B. Ya. Shapiro, and M. Shvartser, Phys. Rev. Lett. **80**, 2441 (1998); I. Aranson, A. Gurevich, and V. Vinokur, *ibid.* **87**, 067003 (2001).

[16] C. Villard, C. Peroz, and A. Sulpice, J. Low Temp. Phys. **131**, 957 (2003).

[17] B. Kalisky, G. Koren, A. Shaulov, Y. Yeshurun, and R. P. Huebener (unpublished).

[18] L. Burlachkov, D. Giller, and R. Prozorov, Phys. Rev. B **58**, 15067 (1998).

[19] D. Zwillinger, *Handbook of Differential Equations*, 3rd ed. (Academic Press, Boston, 1997), p. 424.

[20] L. D. Landau and E. M. Lifshitz, *Fluid Mechanics*, Course of Theoretical Physics Vol. 6 (Pergamon Press, New York, 1980).

[21] M. Aravind and P. C. W. Fung, Meas. Sci. Technol. **10**, 979 (1999).